Table 1. Summary of mechanical properties for PVA and its nanocomposites. The data are mean ± SD. The tensile strengths reported were obtained using both a commercially available servohydraulic test system and a custom in-house–built tensiometer (fig. S2). The moduli were obtained using the custom-built tensiometer. *N* indicates the minimum number of experimental data points that we used in the statistical calculations.

Sample type (*N*)	Tensile strength σ_{UTS} (MPa)	Modulus *E′* (GPa)	Ultimate strain ε (%)
PVA (5)	40 ± 4	1.7 ± 0.2	35 ± 4
PVA with GA (5)	40 ± 10	2.0 ± 0.5	3.3 ± 1.3
PDDA (5)	12 ± 4	0.2 ± 0.03	48 ± 9
PDDA-MTM (*)	100 ± 10	11 ± 2	10 ± 2
PVA/MTM (5)	150 ± 40	13 ± 2	0.7 ± 0.2
PVA/MTM with GA (5)	400 ± 40	106 ± 11	0.33 ± 0.04

*Data are the previously published results by Tang *et al.* (*15*) for 1.2-to-4.9–μm–thick (50 to 200 bilayers) samples tested at relative humidity of 32%.

We believe that the explanation of these results lies in the effective stiffening of the PVA matrix (due to constrained motion of the polymer chains) because of its close proximity to and many interactions with the MTM platelets. The evidence of this reinforcement mechanism comes from differential scanning calorimetry (DSC) analysis (Fig. 3, C to F), which shows suppression of the thermal motion of the PVA when it is constrained between dispersed nanoplatelets. This effect should result in a shift in glass transition temperature (T_g) toward the higher values. However, the overall suppression of motion makes the actual T_g of the polymer not very well defined for such systems, as can be seen in the width of the corresponding DSC peaks. A similar effect can be seen from a comparison of polymer melting temperatures (T_m) between pure PVA (Fig. 4C) and PVA/MTM (Fig. 4E). Whereas the T_m in PVA is sharp and very well defined, PVA/MTM shows strong suppression and broadening of the peak. An additional consequence of such stiffening is that traditional theories of composite mechanics using the bulk properties of pure polymers are difficult to apply to composites with high contents of a uniformly distributed inorganic phase. Mechanical-property enhancement in the GA cross-linked PVA/MTM is a result of an increase in the likelihood that a polymer chain in the PVA/MTM with GA system interacts strongly with two or more clay platelets, thereby improving the particle-to-matrix-to-particle load-transfer process over that in the PVA/MTM system.

In conclusion, reinforcement in polymer-nanoplatelet systems such as PVA/MTM is the result of several mechanisms operating at the nanoscale. The degree of structural organization (afforded by the LBL process) of the clay platelets in the composite maximizes the number of polymer/MTM interactions and constrains the polymer-chain motion, which results in a highly efficient load transfer between the polymer phase and the stiff MTM platelets.

References and Notes

1. M. M. J. Treacy, T. W. Ebbesen, J. M. Gibson, *Nature* **381**, 678 (1996).
2. M.-F. Yu *et al.*, *Science* **287**, 637 (2000).
3. O. Breuer, U. Sundararaj, *Polym. Compos.* **25**, 630 (2004).
4. G. Van Lier, C. Van Alsenoy, V. Van Doren, P. Geerlings, *Chem. Phys. Lett.* **326**, 181 (2000).
5. A. Sturcova, G. R. Davies, S. J. Eichhorn, *Biomacromolecules* **6**, 1055 (2005).
6. O. L. Manevitch, G. C. Rutledge, *J. Phys. Chem. B* **108**, 1428 (2004).
7. J. J. Mack *et al.*, *Adv. Mater.* **17**, 77 (2005).
8. M. A. S. A. Samir, F. Alloin, A. Dufresne, *Biomacromolecules* **6**, 612 (2005).
9. S. S. Ray, M. Okamoto, *Prog. Polym. Sci.* **28**, 1539 (2003).
10. E. P. Giannelis, *Adv. Mater.* **8**, 29 (1996).
11. G. Lagaly, *Appl. Clay Sci.* **15**, 1 (1999).
12. G. Decher, *Science* **277**, 1232 (1997).
13. A. A. Mamedov *et al.*, *Nat. Mater.* **1**, 190 (2002).
14. M. Olek *et al.*, *Nano Lett.* **4**, 1889 (2004).
15. Z. Tang, N. A. Kotov, S. Magonov, B. Ozturk, *Nat. Mater.* **2**, 413 (2003).
16. E. R. Kleinfeld, G. S. Ferguson, *Science* **265**, 370 (1994).
17. P. T. Hammond, *Adv. Mater.* **16**, 1271 (2004).
18. C. Jiang, V. V. Tsukruk, *Adv. Mater.* **18**, 829 (2006).
19. Z. Tang, Y. Wang, P. Podsiadlo, N. A. Kotov, *Adv. Mater.* **18**, 3203 (2006).
20. P. Podsiadlo, Z. Tang, B. S. Shim, N. A. Kotov, *Nano Lett.* **7**, 1224 (2007).
21. P. Podsiadlo, Z. Liu, D. Paterson, P. B. Messersmith, N. A. Kotov, *Adv. Mater.* **19**, 949 (2007).
22. A. A. Bonapasta, F. Buda, P. Colombet, *Chem. Mater.* **12**, 738 (2000).
23. M. Nagy, E. Wolfram, T. Varadi, *Prog. Colloid Polym. Sci.* **60**, 138 (1976).
24. D. Braun, E. Walter, *Colloid Polym. Sci.* **258**, 795 (1980).
25. Y. Guan *et al.*, *J. Phys. Chem. B* **110**, 13484 (2006).
26. A. Mamedov, J. Ostrander, F. Aliev, N. A. Kotov, *Langmuir* **16**, 3941 (2000).
27. M. Cheng, W. Chen, T. Weerasooriya, *J. Eng. Mater. Technol.* **127**, 197 (2005).
28. C. Y. Yue, G. X. Sui, H. C. Looi, *Compos. Sci. Technol.* **60**, 421 (2000).
29. A. M. Hindeleh, S. Abdo, *Polym. Commun.* **30**, 184 (1989).
30. A. B. Dalton *et al.*, *Nature* **423**, 703 (2003).
31. J. S. Bergstrom, M. C. Boyce, *Rubber Chem. Technol.* **72**, 633 (1999).

32. P.P. thanks the Fannie and John Hertz Foundation for support of his work through graduate fellowship. The authors thank Y. Elkasabi for help with FTIR spectroscopy and ellipsometry measurements; the staff of the Electron Microscopy Analysis Laboratory (Univ. of Michigan) and NSF (grant DMR-0320740); the Air Force Office of Scientific Research program on multifunctional materials (grant FA9550-05-1-043), and the U.S. Office of Naval Research (grant N00014-06-1-0473) for financial support.

Supporting Online Material

www.sciencemag.org/cgi/content/full/318/5847/80/DC1
Materials and Methods
Figs. S1 to S10
References

28 March 2007; accepted 4 September 2007
10.1126/science.1143176

Major Australian-Antarctic Plate Reorganization at Hawaiian-Emperor Bend Time

J. M. Whittaker,[1]* R. D. Müller,[1] G. Leitchenkov,[2] H. Stagg,[3] M. Sdrolias,[1] C. Gaina,[4] A. Goncharov[3]

A marked bend in the Hawaiian-Emperor seamount chain supposedly resulted from a recent major reorganization of the plate-mantle system there 50 million years ago. Although alternative mantle-driven and plate-shifting hypotheses have been proposed, no contemporaneous circum-Pacific plate events have been identified. We report reconstructions for Australia and Antarctica that reveal a major plate reorganization between 50 and 53 million years ago. Revised Pacific Ocean sea-floor reconstructions suggest that subduction of the Pacific-Izanagi spreading ridge and subsequent Marianas/Tonga-Kermadec subduction initiation may have been the ultimate causes of these events. Thus, these plate reconstructions solve long-standing continental fit problems and improve constraints on the motion between East and West Antarctica and global plate circuit closure.

A long-standing controversy in global tectonics concerns the ultimate driving forces that episodically cause major plate tectonic reorganizations. Proponents of "top-down" mechanisms [e.g., (*1*, *2*)] argue that plates themselves drive instabilities of the plate-mantle system, whereas others [e.g., (*3*)] have argued that major mantle overturns drive plate tectonic punctuations. The most prominent manifestation of this controversy is the Hawaiian-Emperor sea-

mount chain bend (HEB) (*4*). Whereas there is ample evidence from hotspot trails (*5*), paleomagnetism (*4*), geodynamic models (*6*), and intraplate volcanism (*7*) to support a mantle flow mechanism, there has been a lack of evidence for a plate reorganization at the original age of 43 million years ago (Ma) (*8*) proposed for the HEB (*9*). However, Wessel *et al*. (*10*) recognized that the recent redating of bend initiation to ~50 Ma (*11*) correlates the HEB with major tectonic events from around the Pacific, such as South Pacific triple-junction reorganization at magnetic anomaly chron 22-21 (49.7 to 47.9 Ma) (*12*), Farallon-Pacific fracture zone bends at magnetic anomaly chron 24-21 (53.3 to 47.9 Ma) (*13*), and the direction change and proposed halt of Pacific–Kula plate spreading at magnetic anomaly chron 24-20/19 (53.3 to 43.8/41.5 Ma) (*14*).

The southeast Indian Ocean is a region where a plate event contemporaneous with a major Pacific plate reorganization might be expected, but a historical paucity of magnetic anomaly data close to the Australian and Antarctic margins, combined with slow initial spreading rates, has resulted in poorly constrained plate fits before 50 Ma (*15*). Published reconstructions that assume a north-south spreading direction between Australia and Antarctica result in large overlaps between the South Tasman Rise and Cape Adare (*15*), and offsets in matching Australia-Antarctic geological terranes (*16*). Magnetic anomaly identifications, related to India-Antarctica spreading at 126 to 130 Ma (*17*), have been identified north of the Bruce Rise, Antarctica (Fig. 1), which results in the tectonically problematic juxtaposition of India-Antarctica–related magnetic anomalies between Australia and Antarctica when the Naturaliste Plateau is reconstructed to the north of the Bruce Rise (*15*). These problems indicate that Australia has been placed too far west with respect to a fixed Antarctica and that it is incorrect that the Perth and Vincennes fracture zones are conjugates (*15*). Two Australian-Antarctic fracture zone fabrics can be clearly identified from gravity anomaly data (Fig. 1): a northwest-southeast fabric on ocean floor older than chron 34 (83 Ma) and a north-south fabric on ocean crust younger than chron 21 (47.9 Ma). The model by Tikku and Cande (*15*) implies that the change in spreading direction resulting in these different fabrics occurred before chron 34 (83 Ma). Instead, we test the hypothesis that the Perth Fracture Zone is conjugate to a fracture zone, here named the Perth South Fracture Zone (Fig. 1), resulting in reconstruction of the Bruce Rise to the west of the Naturaliste Plateau. For our revised model, we investigate whether gravity

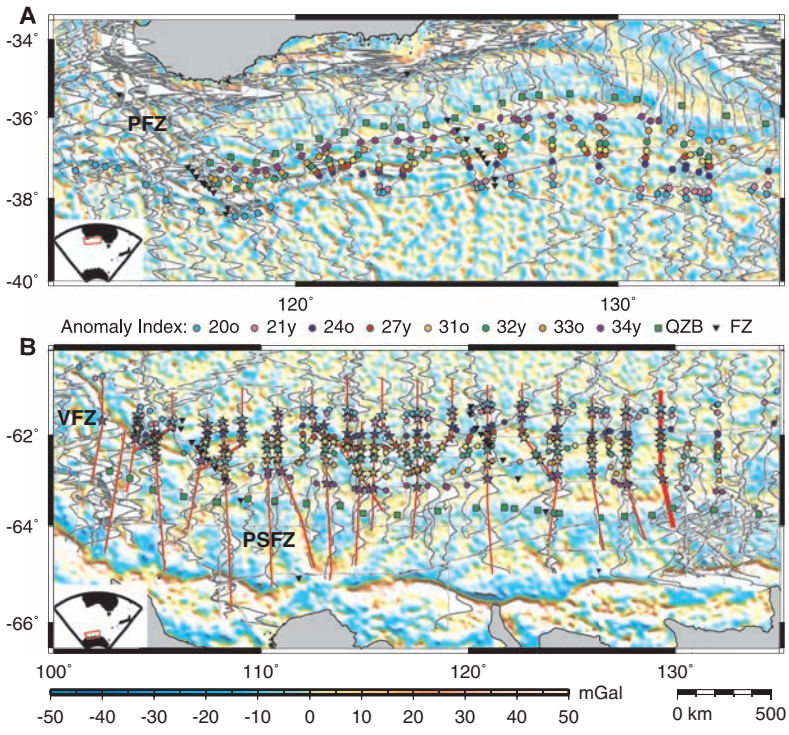

Fig. 1. Low-pass filtered (downward continued to the sea floor) 2-min gravity anomaly grid (*18*, *28*) for (**A**) Southern Australia and (**B**) East Antarctica (inset shows locations). Overlaid are ship tracks (gray lines), magnetic anomaly wiggles (black lines filled with white), gravity anomaly picks [squares, QZB (Quiet Zone Boundary)], fracture zone picks (inverted triangles, FZ), and magnetic anomaly picks [stars, this study; circles, Tikku and Cande (*15*)] used in this paper. Red lines in (B) are Geoscience Australia and Russian shiptracks (see main text), and bold red is shiptrack GA-22825 (fig. S1). PFZ, Perth Fracture Zone; PSFZ, Perth South Fracture Zone; and VFZ, Vincennes Fracture Zone.

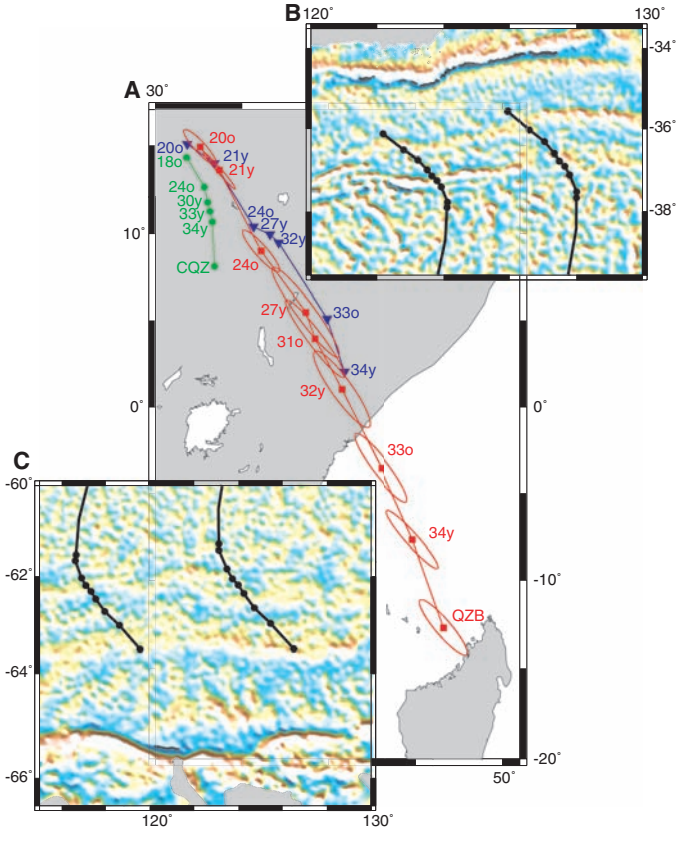

Fig. 2. (**A**) Poles about which Australia is restored to Antarctica based on calculated angles of rotation (finite poles of rotation) with 95% confidence interval ellipses. Red squares and red error ellipses represent our new rotation poles, inverted triangles are Tikku and Cande's (*15*) rotation poles, and green circles are Royer and Rollet's (*29*) rotation poles. (**B**) South Australian margin and (**C**) East Antarctic margin, downward continued gravity anomaly with fit of tectonic flowlines resulting from our new model. Tectonic flowlines are constructed for stage rotations between magnetic chrons shown in Fig. 1.

[1]EarthByte Group, School of Geosciences, University of Sydney, Sydney 2006, Australia. [2]VNII Okeangeologia (Antarctic Branch), St. Petersburg 190121, Russia. [3]Geoscience Australia, Canberra 2601, Australia. [4]Center for Geodynamics, Norwegian Geological Survey, Trondheim 7491, Norway.

*To whom correspondence should be addressed: E-mail: j.whittaker@geosci.usyd.edu.au

anomalies (*18*) permit a change in spreading direction at a younger time, resulting in a longer period of oblique relative motion than previously assumed.

New magnetic anomaly identifications made with recently acquired high-quality magnetic data in the Bruce Rise area (90° to 115°E) and along the Terre Adelie and Wilkes Land margins (115° to 132°E) were integrated with earlier identifications (*15*) (Fig. 1 and table S2). The motion of a tectonic plate can be described by a rotation angle about a virtual axis that passes through the center of the Earth and intersects its surface (finite pole of rotation). We used the combined fracture zone and magnetic anomaly identifications (Fig. 1) to define a new set of plate boundaries and compute well-constrained finite rotations and 95% uncertainty intervals (Fig. 2 and tables S3 and S4) that describe our new plate motion history for Australia and East Antarctica.

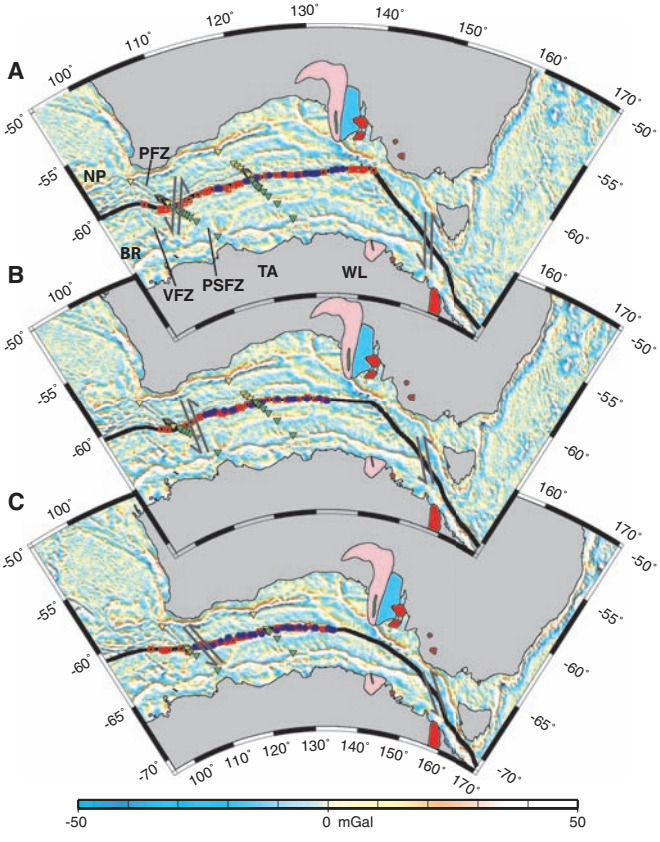

Fig. 3. Australia-Antarctica reconstructions based on our rotations at three stage boundaries: (**A**) 47.9 Ma, chron 21; (**B**) 61 Ma, chron 27; and (**C**) 83 Ma, chron 34. All magnetic chron ages are based on the time scale of Cande and Kent (*30*). Underlying image shows downward continued gravity anomalies. At 83 Ma, the Naturaliste Plateau (NP) is located to the east of the Bruce Rise (BR), there is no overlap between southeast Australia and Antarctica, and the Australian/Antarctic geological provinces align. Dark gray arrows show direction of motion of Australia and Antarctica for stages chron 21 to chron 18, chron 27 to chron 21, and chron 34 to chron 27 in (A), (B), and (C), respectively. Magnetic anomaly identifications for Australia and Antarctica for each reconstruction time are shown as red circles and black squares, respectively. Inverted triangles are fracture zone identifications for each chron older than the time of reconstruction. Geological provinces are as follows: pink, Neoarchean basement [~2.5 billion years ago (Ga)]; green, Paleoproterozoic basin (~1.69 Ga); light blue, metasediments (~2 Ga); and red, plutonic belt (~500 Ma) (*16*, *31*, *32*). WL, Wilkesland; TA, Terra Adelie; PFZ, Perth Fracture Zone; PSFZ, Perth South Fracture Zone; and VFZ, Vincennes Fracture Zone.

Our new plate reconstructions resolve long-standing continental and geological terrane fit problems with Australia, relative to Antarctica, positioned ~500 km east of previous reconstructions at 83 Ma (Fig. 3), and provide improved constraints on the motion between East and West Antarctica and global plate circuit closure.

When combined with geological evidence for relative plate motion changes around the Pacific, our reconstructions provide strong evidence for a major plate reorganization, which we argue was initiated by the subduction of the Izanagi-Pacific (I-P) ridge—a "top-down" mechanism. Circum-Pacific fracture zone bends document relative plate motion changes precipitated by the I-P ridge subduction, whereas the prominent HEB formed through a combination of altered Pacific plate motion and the well-documented deceleration of Pacific mantle (*4*, *6*).

We present a new plate reconstruction for the western Pacific (Fig. 4) based on matching isochrons and a set of simple assumptions (table S5). In our plate model, mid-ocean ridge subduction beneath southern Japan occurs at 60 to 55 Ma, 20 million years later than proposed for Kula-Pacific (*19*) or Farallon-Izanagi (*20*) ridge subduction. The difference arises because I-P spreading ceases in previous models after 110 Ma, whereas our model incorporates continued spreading until the I-P ridge subducts beneath eastern Asia at 60 to 55 Ma. Cessation of spreading at the I-P ridge between 110 and 80 Ma is unlikely because the Izanagi plate was undergoing rapid motion, driven by net slab-pull force, from the north-northwest (*21*), immediately before the proposed spreading cessation.

Metamorphism of the Ryoke Belt in southern Japan has previously been attributed to Kula–Pacific ridge subduction at 85 Ma (*19*), but the high-temperature/low-pressure Ryoke Belt cannot be uniquely linked to a ridge subduction event (*22*). Unreasonably high spreading rates of 35 to 40 cm/year during the Cretaceous Normal Superchron between the Pacific and Izanagi plates would be necessary to subduct the I-P ridge at 85 Ma, which is more than double the fastest current spreading rate globally [~15 cm/

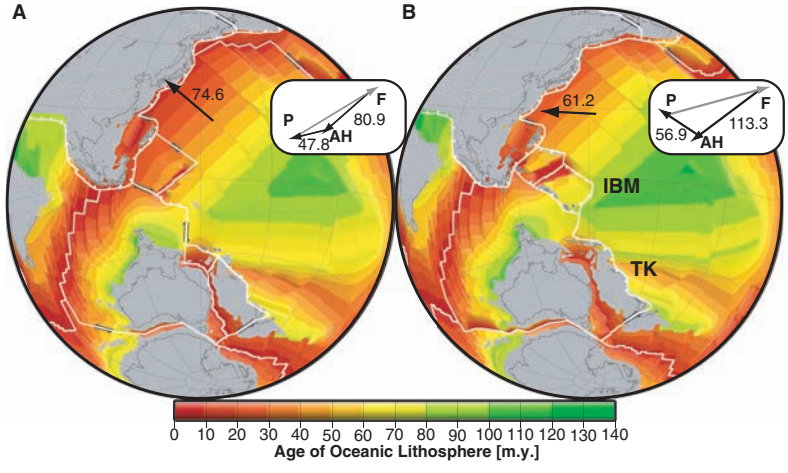

Fig. 4. Reconstructed oceanic crustal age grids at two time slices (**A**) 55 Ma and (**B**) 45 Ma. Black arrows (in mm/year) show western Pacific (30°N, 150°E) plate motion over the stages 60 to 50 Ma and 50 to 40 Ma, respectively. (Inset) Vectors (in mm/year) (same 10-Ma stages) show motion of the eastern Pacific (30°N, 240°E) (P) and Farallon (F) plates relative to fixed African hotspots (AH) over the period 60 to 50 Ma and 50 to 40 Ma. Eastern and western Pacific directions and changes in plate motion are substantially different. Geographical location of poles (latitude, longitude) about which rotations (angle) describing Pacific plate motion relative to an African hotspot reference frame are 55.0°N, –118.4°W, –7.90° and 59.4°N, –19.3°W, –5.52° at 60 to 50 Ma and 50 to 40 Ma, respectively. The resultant relative plate motions between the Pacific and Farallon plates show that our model explains the shape of the Pacific-Farallon fracture zone bend as well as the HEB. TK, Tonga-Kermadec subduction zone; IBM, Izu-Bonin-Marianas subduction zone. m.y., millions of years.

year between the Pacific and Nazca plates (*23*)]. We propose that subparallel subduction of the I-P mid-ocean ridge beneath Japan at 60 to 55 Ma resulted in nearly simultaneous slab break-off along the length of the Japanese trench (~2700 km). Geological observations from southern Japan support subduction of the I-P ridge and subsequent slab break-off at 60 to 55 Ma. Evidence includes cessation of a major accretion phase in the Late Cretaceous (*24*), emplacement of the Okitsu Melange due to subduction of hot, buoyant material at 55 Ma (*24*), and cross-cutting fault fabrics that indicate a counterclockwise rotation in relative plate motions between Eurasia and the I-P plate, which are also consistent with paleothermal and paleopressure data, between 55 and 34 Ma (*25*).

Rapid subduction of the I-P ridge, over a vast distance, triggered a chain reaction of tectonic plate reorganizations. With complete subduction of the I-P ridge at 55 Ma, forces acting on the Pacific changed from ridge-push to slab-pull, which changed Pacific absolute plate motions from northwest to west (Fig. 4). The change in Pacific plate motion caused cessation of Tasman Sea spreading at ~52 Ma (*26*). Increased slab pull north of Australia, due to a westerly progression of the subducting Wharton Basin mid-ocean ridge (Fig. 4), changed Australian absolute plate motion from northwest to north. A combination of Australian and Pacific plate motion changes between 53 and 50 Ma initiated both the Tonga-Kermadec (*2*) subduction system and the Izu-Bonin-Marianas subduction systems, which initiated likely before 50 Ma, due to convergence across a fracture zone caused by the Pacific plate motion change (*27*). We suggest that the observed slowdown of sub-Pacific mantle flow at 47 Ma (*4*) was due to progressive impediment of lateral sub-Pacific mantle flow by the descending slabs of the Izu-Bonin-Marianas and Tonga-Kermadec subduction zones.

The observed opposite bend geometries of the Emperor-Hawaii seamount chain and the Pacific-Farallon fracture zones can be explained with combined absolute (relative to a fixed reference frame) and relative plate motions. Clockwise rotation of eastern Pacific absolute plate motion, combined with stable Farallon plate motion (Fig. 4), results in a clockwise bend in Pacific-Farallon fracture zones at 53 to 49 Ma (*16*). In the western Pacific, a counterclockwise change in absolute plate motion, from northwest to west due to Izanagi Ridge subduction (Fig. 4), combined with a sub-Pacific mantle flow slowdown, results in the HEB. This conceptual model is testable via three-dimensional fully dynamic mantle flow simulations.

References and Notes

1. D. L. Anderson, *Science* **293**, 2016 (2001).
2. M. Gurnis, C. Hall, L. Lavier, *Geochem. Geophys. Geosyst.* **5**, Q07001 (2004).
3. S. D. King, J. P. Lowman, C. W. Gable, *Earth Planet. Sci. Lett.* **203**, 83 (2002).
4. J. A. Tarduno *et al.*, *Science* **301**, 1064 (2003).
5. P. Molnar, J. Stock, *Nature* **327**, 587 (1987).
6. B. Steinberger, R. Sutherland, R. J. O'Connell, *Nature* **430**, 167 (2004).
7. C. A. Finn, R. D. Müller, K. S. Panter, *Geochem. Geophys. Geosyst.* **6**, Q02005 (2005).
8. D. A. Clague, G. B. Dalrymple, *U.S. Geol. Surv. Prof. Paper* **1350** (1987).
9. I. O. Norton, *Tectonics* **14**, 1080 (1995).
10. P. Wessel, Y. Harada, L. W. Kroenke, *Geochem. Geophys. Geosyst.* **7**, Q03L12 (2006).
11. W. D. Sharp, D. A. Clague, *Science* **313**, 1281 (2006).
12. S. C. Cande, E. M. Herron, B. R. Hall, *Earth Planet. Sci. Lett.* **57**, 63 (1982).
13. D. W. Caress, H. W. Menard, R. N. Hey, *J. Geophys. Res.* **93**, 2813 (1988).
14. P. F. Lonsdale, *Bull. Geol. Soc. Am.* **100**, 733 (1988).
15. A. A. Tikku, S. C. Cande, *J. Geophys. Res.* **104**, 661 (1999).
16. C. A. Finn, D. Moore, D. Damaske, T. Mackey, *Geology* **27**, 1087 (1999).
17. C. Gaina, R. D. Müller, B. Brown, T. Ishihara, S. Ivanov, *Geophys. J. Int.* **170**, 151 (2007).
18. D. T. Sandwell, W. H. F. Smith, *Geophys. J. Int.* **163**, 79 (2005).
19. D. C. Engebretson, A. Cox, R. G. Gordon, *Geol. Soc. Am. Spec. Pap.* **206**, 1 (1985).
20. C. T. Onishi, G. Kimura, *Tectonics* **14**, 1273 (1995).
21. K. Otsuki, *Island Arc* **1**, 51 (1992).
22. M. Brown, *J. Metamorphic Geol.* **16**, 3 (1998).
23. W. P. Schellart, J. Freeman, D. R. Stegman, L. Moresi, D. May, *Nature* **446**, 308 (2007).
24. S. M. Agar, R. A. Cliff, I. R. Duddy, D. C. Rex, *J. Geol. Soc.* **146**, 893 (1989).
25. J. C. Lewis, T. B. Byrne, *Tectonics* **20**, 548 (2001).
26. C. Gaina *et al.*, *J. Geophys. Res.* **103**, 12413 (1998).
27. C. E. Hall, M. Gurnis, M. Sdrolias, L. L. Lavier, R. D. Müller, *Earth Planet. Sci. Lett.* **212**, 15 (2003).
28. W. H. F. Smith, D. T. Sandwell, *J. Geophys. Res.* **99**, 21803 (1994).
29. J.-Y. Royer, N. Rollet, *Aust. J. Earth Sci.* **44**, 543 (1997).
30. S. C. Cande, D. V. Kent, *J. Geophys. Res.* **100**, 6093 (1995).
31. G. Duclaux, P. Rey, S. Guillot, R. P. Ménot, *Geology* **35**, 715 (2007).
32. R. P. Ménot *et al.*, in *Antarctica: A Keystone in a Changing World—Online Proceedings of the 10th ISAES,* A. K. Cooper et al., Eds. (USGS Open-File Rep. 2007-1047, Short Research Paper 048, 2007).

33. We thank W. Smith for providing the downward continued gravity grid. Reviews by M. Gurnis and S. Cande, as well as detailed comments on early versions of the manuscript by P. Wessel, A. Dutkiewicz, and J. Stock, improved the manuscript considerably. We acknowledge the Ministry of Natural Resources of the Russian Federation and Geoscience Australia, who funded collection of some of the new marine magnetic data used in this work.

Supporting Online Material

www.sciencemag.org/cgi/content/full/318/5847/83/DC1
Fig. S1
Tables S1 to S5
References

13 April 2007; accepted 3 September 2007
10.1126/science.1143769

Absence of Cooling in New Zealand and the Adjacent Ocean During the Younger Dryas Chronozone

Timothy T. Barrows,[1]* Scott J. Lehman,[2] L. Keith Fifield,[1] Patrick De Deckker[3]

As the climate warmed at the end of the last glacial period, a rapid reversal in temperature, the Younger Dryas (YD) event, briefly returned much of the North Atlantic region to near full-glacial conditions. The event was associated with climate reversals in many other areas of the Northern Hemisphere and also with warming over and near Antarctica. However, the expression of the YD in the mid- to low latitudes of the Southern Hemisphere (and the southwest Pacific region in particular) is much more controversial. Here we show that the Waiho Loop advance of the Franz Josef Glacier in New Zealand was not a YD event, as previously thought, and that the adjacent ocean warmed throughout the YD.

The Younger Dryas (YD) event was originally recognized in Northern Europe and the adjacent North Atlantic Ocean as an abrupt return to near full-glacial conditions between 11,000 and 10,000 radiocarbon (^{14}C) years ago, an interval defined as the YD chronozone (*1*). Layer counting of Greenland ice cores (*2*), tree ring counts (*3*), and calibration of the ^{14}C time scale (*4*) now place the event between ~12,900 and ~11,600 calendar years before the present (cal yr B.P.). Evidence for teleconnected reversals of climate at this time occurs widely in the Northern Hemisphere (*5*), whereas the transfer of the Greenland climate stratigraphy to Antarctic ice cores via measurements of globally well-mixed atmospheric CH_4 trapped within the ice show clearly that a deglacial reversal of climate warming in Antarctica [the Antarctic Cold Reversal (ACR)] ended just as the Northern Hemisphere YD began (*6*). The latter is consistent with an antiphased relation of climate between Greenland and Antarctica seen earlier

[1]Department of Nuclear Physics, Research School of Physical Sciences and Engineering, The Australian National University, Canberra, ACT 0200, Australia. [2]Institute of Arctic and Alpine Research and Department of Geological Sciences, University of Colorado, Boulder, CO 80309, USA. [3]Department of Earth and Marine Sciences, The Australian National University, Canberra, ACT 0200, Australia.

*To whom correspondence should be addressed. E-mail: Tim.Barrows@anu.edu.au